MDPH396 Research Report

A Preliminary Investigation of Lymphocyte-Sparing Radiation Therapy

Charles-Etienne Gaudet

Fall 2025

Abstract

Radiation-induced lymphopenia is a frequent complication of external-beam radiation therapy, yet circulating lymphocytes are not taken into account during treatment planning. In this project, a computational pipeline combining automated organ segmentation, hematological dose calculation, and lymphocyte survival modelling was used to compare two radiation plans for lung cancer: an initial plan following MUHC guidelines and an optimized plan following the stricter LymphoTEC dose constraints. Absolute lymphocyte count evolution was modelled for both plans, showing that the optimized plan reduced anticipated lymphocyte depletion, consistent with decreased irradiation of highly vascularized organs. These results, which were statistically significant across repeated paired simulations, provide a preliminary investigation of the potential benefit of lymphocyte-sparing radiation therapy.

Contents

1 Introduction

1.1 Background

1.1.1 Lymphocytes

Lymphocytes are a type of white blood cell of utmost importance to the immune system, and account for up to 40% of the total number of immune cells [1]. They play a central role in adaptive immunity by enabling targeted immune responses and long-term immune memory [2].

They can be present either as circulating lymphocytes or non-circulating lymphocytes. Non-circulating lymphocytes are located in lymphocyte-producing organs such as lymph nodes and tonsils (41%), the spleen (15%), bone marrow (11%), the thymus in children (11%), gut-associated lymphoid tissue (4%), and other tissues ($\approx$ 15%) [3]. On the other hand, circulating lymphocytes are consistently moving through the blood and lymphatic system, being exchanged between tissues and lymphoid organs (including lymphocyte-producing organs), where they are produced or transiently reside. Circulating lymphocytes are carried throughout the body to serve their role in the immune system. Comprising only around 2.2% of the total lymphocyte count [3], circulating lymphocytes are the most radiosensitive [4].

An individual's lymphocyte count is usually expressed as Absolute Lymphocyte Count (ALC) and is measured through laboratory measurements of the number of lymphocytes per μL of blood. As they travel through the blood, circulating lymphocytes are transiently present in vascular organs at rates proportional to the incoming and exiting blood flow in each organ. Patient-specific values for lymphocyte transit fractions (between organs) are difficult to measure, but reference values are publicly available [5].

1.1.2 Lymphocyte Radiosensitivity

In addition to being among the most radiosensitive cell types, circulating lymphocytes are predisposed to initiate apoptosis when irradiated [4]. Exposure to radiation, even in small amounts, may cause DNA damage and initiate apoptosis [4]. Various mathematical models have been developed in the past to predict their radiation-induced behaviour. More recently, studies have extended the commonly used linear-quadratic survival model, and suggested the use of a saturation model to account for a resistant lymphocyte subpopulation, assuming Poisson-like cell survival [6]:

$$S(D) = \left[S_{F_{\text{sat}}}\right]^{1-e^{-\mu D}} \tag{1}$$

Parameters and variables:

D: dose [Gy]

$S(D)$: surviving fraction of lymphocytes at dose D

$S_{F_{\text{sat}}}$: saturation survival fraction, 0.57 ± 0.02

μ: rate of damage accumulation, 2.18 ± 0.35 Gy^{-1}

1.1.3 Lymphopenia and Radiation-Induced Lymphopenia

Lymphopenia is a condition in which an individual's ALC falls below the normal range, resulting in impaired immune function. It is known that radiation therapy and chemotherapy are the main cancer-treatment-related causes of lymphopenia [4]. To quantify its severity, lymphopenia is classified by grades. Table 1.1 summarizes the CTCAE grading thresholds for lymphopenia [7].

Table 1.1: CTCAE v5.0 lymphopenia grading based on ALC [7].

Grade	**ALC (cells/μL)**
1	800–999
2	500–799
3	200–499
4	< 200

Radiation-induced lymphopenia (RIL) is a condition in which lymphopenia presents during or following radiation treatments. Studies have shown that it occurs in 40% to 70% of patients treated by external-beam radiation therapy [8]. The exact mechanism of the condition continues to be studied by the scientific community and remains poorly understood, as radiation is known to have both immuno-stimulatory and immuno-suppressive effects [4].

Although different treatment modulations, such as how the dose is spread in space and time, can affect the occurrence of lymphopenia, previous research has correlated absorbed dose with radiation-induced lymphocyte depletion in lymphocyte-rich organs at risk (LOARs), such as the bone marrow, spleen, and lymph nodes [4].

The high radiosensitivity of circulating lymphocytes has led the scientific community to investigate whether the radiation-induced depletion of these cells is a cause of lymphopenia in patients treated with radiation therapy [4], compared with other factors such as tumour-related immunosuppression and concomitant therapies.

The mechanism through which circulating lymphocytes absorb radiation is more complex than for localized organs owing to their motion. On average, blood is recirculated around the body approximately once every minute [9], and in this way a single circulating lymphocyte may be exposed multiple times during a single treatment fraction. Lymphocyte exposure is therefore influenced not only by the total dose prescribed, but also by the number of and time intervals between radiation beams, dose-rate, total blood volume, cardiac output, tumour site, and other factors, highlighting the complexity of the problem.

ALC, or more precisely the onset of lymphopenia, has been shown to be a prognostic factor and indicator of survival in cancer patients. Severe (CTCAE Grade 3–4) lymphopenia has been associated with increased complications and poor outcomes, such as infection, tumour progression, and metastasis [10]. In a systematic review and meta-analysis of over 13,000 patients, lymphopenia was found to be correlated with a higher risk of death in patients with grade 3–4 lymphopenia compared with grade 0–2 lymphopenia [10].

Despite common skepticism in the medical field regarding the clinical relevance of lymphocyte sparing, Lambin et al. first suggested the use of the "As Low As Reasonably Achievable" principle in 2019 to limit radiation exposure and avoid over-irradiating LOARs and vascular organs [11]. To further investigate lymphocyte-sparing radiation therapy, they also proposed additional data collection during cancer radiation treatments, including dose-volume and dose-rate statistics, as well as ALC monitoring.

1.1.4 Lymphocyte-Rich Organs At Risk and LymphoTEC

In an attempt to minimize the exposure of lymphocytes to radiation, it is reasonable to restrict the dose delivered to LOARs and to vascular organs such as the heart, lungs, and brain, as circulating lymphocytes pass through these organs in the bloodstream and are irradiated while being inside the organ volume (i.e., while the organ itself is receiving dose). As previous studies had examined the correlation between ALC and absorbed dose to relevant organs, a 2022 systematic review of the literature on dose constraints and lymphocyte depletion by Venkatesulu et al., known as LymphoTEC, suggested dose constraints for both LOARs and vascular organs [12]. This represented an important first step toward lymphocyte-sparing radiation therapy. Although these guidelines have yet to be validated by the broader scientific and medical community, they offer a key opportunity to apply the "As Low As Reasonably Achievable" principle in practice.

These guidelines provide volume-at-dose[1] ($D_{x\%}$) or dose-at-volume[2] constraints, where $D_{x\%}$ is a dose defined by a fixed volume fraction and $V_{x\,\mathrm{Gy}}$ is a volume fraction defined by a fixed dose level.

Table 1.2: Suggested LymphoTEC guidelines for vascular organs and LOARs [12].

Organ / Region	**Dose constraints**		
Lung	$D_{\mathrm{mean}} < 12$–14 Gy	$V_5 < 45\%$	$V_{10} < 30\%$
Heart	$D_{\mathrm{mean}} < 5.2$ Gy	$V_5 < 38\%$	$V_{10} < 25\%$
Whole body / EDIC*	EDIC < 4–7 Gy	$D_{\mathrm{mean}}^{\mathrm{body}} < 12$ Gy	$V_{10}^{\mathrm{body}} < 18\%$
Brain	$D_{\mathrm{mean}} < 34$ Gy	$V_{25} < 40\%$	
Spleen	$D_{\mathrm{mean}} < 2.3$ Gy	$V_{20} < 5\%$	
Bone marrow	$D_{\mathrm{mean}}^{\mathrm{thoracic}} < 29$ Gy	$V_{10}^{\mathrm{pelvic}} < 80\%$	$V_{40} < 600$ cc

*EDIC: estimated dose to immune cells.

[1] $D_{x\%}$ represents the dose such that $x\%$ of the volume receives $\geq D$.

[2] $V_{x\,\mathrm{Gy}}$ represents the fraction (in %) of the volume receiving $\geq x$ Gy: $V_{x\,\mathrm{Gy}}(\%) = 100 \times \dfrac{V(D \geq x\,\mathrm{Gy})}{V_{\mathrm{total}}}$.

1.1.5 Previously Developed Hematological Models

Although dose constraints to localized LOARs can easily be implemented through radiation treatment planning, a much more complex problem arises when attempting to deal with circulating lymphocytes due to the dynamical nature of blood flow.

Over the past 15 years, different hematological models were created by the scientific community in an attempt to simulate blood flow, and consequently estimate the hematological dose.

Among the numerous models designed, Molloy et al. first created a simplified whole-body model in 2011 that assumed sinusoidal blood flow between the upper and lower body [13]. However, this framework was not organ-specific, considered a homogeneous blood distribution within the body, and disregarded anatomical features. A decade later, in 2020, Jin et al. used a compartmentalized model taking into account the blood, bone marrow, lymphoid glands, and peripheral tissues [14].

While innovative, these models relied on simplified blood flow and anatomical assumptions, which limited their applicability to patient-specific radiation therapy planning, and therefore accurate hematological dose estimation.

1.1.6 HEDOS

As evident gaps were present in previous frameworks, in 2021, Shin et al. developed the open-source hematological dose (HEDOS) model, a time-dependent computational framework designed to estimate the dose delivered to circulating blood cells during radiation therapy treatments [15].

HEDOS estimates blood dose using a voxel-based approach, relying on the external beam dose distribution together with organ masks to simulate the dose absorbed by blood particles (BPs). The simulation uses two coupled models: the first computes the spatiotemporal distribution of BPs within organs, and the second describes the time-dependent delivery of the radiation field.

The software uses simulated particles (representing a fraction of total blood volume), following a random walk between organs. This stochastic behaviour is governed by a transition matrix containing probabilities and rates of exchange between vascularized organs, modelling blood flow (sex-specific). Based on data published in ICRP Publication 89 [5], it incorporates organ-specific blood flow parameters.

The inputs of the program are as follows:

1. Anatomical data (organ and tumour masks, NumPy array format)
2. Treatment dose map (NumPy array format)
3. Patient characteristics (sex, cardiac output)
4. Tumour information (tumour site, relative perfusion, relative blood density, tumour fraction of the affected organ)
5. Treatment parameters (beam-on time, irradiation intervals)
6. Simulation parameters (number of simulated particles)

Time dependence is fundamental to accurately estimate the hematological dose, as BPs can circulate around the body and travel again through an irradiated organ multiple times during a single fraction, accumulating more dose than if the simulation was performed on a static system. HEDOS therefore takes into account dose-rate/beam-on time.

As HEDOS works with data from ICRP Publication 89, it assumes that all patients of the same sex carry an identical blood flow distribution, irrespective of morphological features; it outputs patient-specific blood dose from population-averaged blood flow. It additionally works with organ-level circulation of blood, and not physical exchange vessels.

The primary output of HEDOS is a blood dose array in which each entry corresponds to the dose accumulated by a simulated blood particle during a fraction. This subsequently allows statistical analysis of the hematological dose from the distribution of this array (such as mean dose). Hence the number of simulation particles only affects precision and not total blood dose.

1.2 Problem Definition and Objectives

As lymphopenia is known to reduce the survival rate of cancer patients, it is of interest to attempt to limit its occurrence by investigating the reduction of radiation exposure to lymphocytes, following the "As Low As Reasonably Achievable" principle.

Using LymphoTEC, which suggests dose constraints to LOARs and vascular organs, and with the help of HEDOS to predict the absorbed blood dose, it is now possible to combine and apply these tools to investigate the achievability of lymphocyte-sparing radiation therapy through treatment replanning.

The objective of this work was to evaluate whether such replanning can reduce blood dose while maintaining clinically acceptable tumour dose coverage, and to analyze the resulting trade-offs in dose distribution.

2 Methods

A CT scan from a single patient was acquired from a previous McGill study and accessed through a public cancer patient dataset [16]. The patient case was randomly selected from the dataset.

2.1 Data and Imaging

2.1.1 Segmentation

The CT scan was segmented using the open-source Python tool TotalSegmentator [17, 18]. A total of 54 anatomical structures were contoured (Table A.1), including vascular organs, LOARs, and other neighbouring organs. Following the automated segmentation, manual corrections were carried out in the Eclipse treatment planning system (Varian Medical Systems, Palo Alto, CA) to ensure accurate organ delimitation, thereby improving organ-dose calculations. The output

data for these vascular organs, LOARs, and neighbouring structures were converted into three-dimensional masks (Table A.1).

2.1.2 Data Handling and Organization

Since this segmentation resulted in a large number of individual organ masks, additional data organization was required to manage structures consistently throughout the project.

To simplify organ name handling, a dictionary of organs to be segmented was implemented (Figure 1a).

Similarly, because HEDOS and LymphoTEC require different masks containing common structures (e.g. a single bone marrow mask in HEDOS versus separate pelvic and thoracic bone marrow masks in LymphoTEC), a second dictionary was defined to list structures needing to be merged for dose constraint evaluation (Figure 1b).

Figure 1: Python dictionaries used to define organ groupings in the analysis pipeline. ORG_SYSTEMS lists anatomical systems used for organization, while GROUPS defines structures merged for dose evaluation and modelling.

(a) ORG_SYSTEMS (excerpt)

```
ORG_SYSTEMS = {
  "abdominal": [
      "liver", "spleen",
      "stomach", ...
  ],
  "cardiothoracic": [
      "heart", "esophagus",
      "pulmonary_vein", ...
  ],...}
```

(b) GROUPS (excerpt)

```
GROUPS = {
  "lung": [
      "lung_upper_lobe_left",
      "lung_lower_lobe_left", ...
  ],
  "bone_marrow_pelvic": [
      "sacrum", "hip_left",
      "hip_right", ...
  ],...}
```

2.1.3 Tumour Generation

Two lung tumours, representing two cases of T1- and T3-stage lung cancer (size-based [19]), were then manually drawn at similar locations in the right lung cavity, each in different copies of the same CT. To simplify contouring and later radiation planning, a single larger tumour was drawn to represent a more severe case, instead of multiple separate tumour nodules (as both can represent a T3-stage disease [19]).

2.1.4 Data Conversion and Automation

With all anatomical data gathered, it remained to convert the whole dataset into NumPy format, as required for the HEDOS input. To achieve this, a fork of the original HEDOS project, which introduced DICOM conversion for contoured structures [20], was modified to support filled-polygon structures (i.e., volumetric masks when rendered). All scripts were run in Python using open-source software libraries SimpleITK [21] and pydicom [22], and the resulting data were exported to `.npy` arrays.

All of the data handling methods mentioned in this subsection were automated into two scripts to handle CT loading, structure handling, dictionary-based mask merging, and the export of all CT and organ masks into NumPy format to prepare for subsequent steps.

2.2 Treatment Planning and Dose Constraints

Two treatment plans were created for comparison. An initial plan followed the MUHC guidelines [23], as described in Table 2.1, while an optimized plan followed the stricter LymphoTEC guidelines specified in Table 1.2.

Table 2.1: MUHC dose constraints for lung radiation therapy (60 Gy in 30 fractions) [23].

Structure	**Constraint**
PTV	$V_{100\%} \geq 95\%$
Spinal cord	Max < 48 Gy
Spinal cord PRV5	Max < 50 Gy
Lungs – PTV	$V_{20\text{Gy}} < 30\%$
Esophagus	$V_{60\text{Gy}} < 33\%$
Heart	$V_{60\text{Gy}} < 33\%$
	$V_{35\text{Gy}} < 50\%$

Both plans were generated using a VMAT technique consisting of two partial arcs from -262° to 180°, with the tumour used as the isocenter, and delivered with 6 MV photons on a Varian STX linear accelerator. A total of 30 fractions were planned, with each fraction delivered in two irradiation periods of 70 s, separated by a 20 s break.

Each plan's DVHs and tumour dose metrics were saved for later comparison.

2.3 HEDOS, Blood Dose, and Lymphocyte Modelling

2.3.1 HEDOS and Blood Dose

Each plan was simulated through HEDOS using 12 independent Monte-Carlo resimulations of the same single-fraction irradiation scenario. These runs were performed solely to quantify stochastic variability and do not correspond to distinct clinical treatment fractions.

The number of simulation particles was set to 20,000, which provided stable stochastic simulations while remaining time-efficient, and the simulation parameters were kept constant between runs and between plans. For each of the 12 simulations, a blood dose array was extracted, consisting of 20,000 entries specifying the dose absorbed by each simulation particle for a single fraction, and all arrays were saved.

2.3.2 Lymphocyte Modelling

Lymphocyte depletion and repopulation were initially modeled based on the framework proposed by McCullum et al. in 2022 [24]. Through daily iterations of a survival probability function, the ALC for each subsequent day was computed based on the previous one, taking into account a linear-quadratic (LQ) apoptosis model for cells exposed to radiation and exponential repopulation:

$$ALC_{t+1} = ALC_t \left[\underbrace{\sum_i f_{d_i} e^{-\alpha d_i}}_{\text{Radiation cell kill}} + \underbrace{\left(1 - e^{-\sigma\left(1-\frac{ALC_t}{ALC_0}\right)}\right)}_{\text{Recovery}} \right] \tag{2}$$

where ALC_t: lymphocyte count at day t, ALC_0: baseline value,
d_i: dose to the i^{th} blood particle, f_{d_i}: fraction of particles at dose d_i,
α: radiosensitivity, σ: recovery parameter.

However, at high radiation doses, this model predicted the ALC to approach zero, inconsistent with some lymphocytes being radio-resistant.

In 2023, an extension to the LQ model was proposed by Pham et al. [6]. This model (Eq. 1) included a saturation factor and showed more accurate modelling of in-vitro unstimulated lymphocytes' (i.e. circulating lymphocytes) survival after irradiation, as it allowed radio-resistance to be taken into account.

While the McCullum et al. framework provides the overall structure of the lymphocyte model, the radiation cell-kill term was replaced in the present work to include a saturation-based apoptosis function given by Eq. 1, yielding the following hybrid model:

$$ALC_{t+1} = ALC_t \left[\underbrace{\frac{1}{N}\sum_{i=1}^{N} (S_{\text{Fsat}})^{1-e^{-\mu d_i}}}_{\substack{\text{Mean per-fraction survival } \bar{S} \\ \text{(constant for a given dose array)}}} + \underbrace{\left(1 - e^{-\sigma\left(1-\frac{ALC_t}{ALC_0}\right)}\right)}_{\text{Recovery}} \right] \tag{3}$$

where ALC_t: ALC at day t, ALC_0: baseline value,
d_i: dose to the i^{th} blood particle, N: number of simulation particles,
μ: radiosensitivity parameter (Pham study), σ: recovery parameter,
S_{Fsat}: saturation survival constant.

2.3.3 Application of the Model

As done in the McCullum et al. study, a treatment schedule was defined as daily irradiation for five consecutive weekdays followed by a two-day break, for a total of 30 fractions.

For each of the 12 Monte-Carlo simulations of the same single-fraction scenario (not independent treatment fractions), the survival function was applied to the corresponding blood-dose array, and the resulting per-simulation survival values were averaged to yield a single survival factor and its associated standard error of the mean (SEM).

This survival factor was applied at each fraction to update ALC_t, assuming an identical per-fraction dose distribution and therefore a constant mean blood dose absorption across all 30 fractions.

Uncertainties arising from the SEM and from parameters in the mathematical model were propagated to each predicted ALC_t to form a 95% confidence interval (Appendix B).

Whereas McCullum et al. varied the dose-rate to investigate changes in blood dose, in this project, distinct treatment plans were compared under identical delivery conditions and simulation parameters.

2.3.4 Outcome Metrics and Statistics

To assess lymphocyte-sparing effects, the nadir ALC, $\mathrm{ALC}_{\mathrm{min}}$, defined as the lowest predicted lymphocyte value over the treatment course was recorded. More precisely, its difference between treatments $|\Delta\mathrm{ALC}_{\mathrm{min}}|$ was examined.

In addition, the maximum sparing difference between plans $|\Delta\mathrm{ALC}|_{\mathrm{max}}$ and the day on which it occurred were evaluated, corresponding to the time point at which the predicted ALC difference between plans was greatest.

Finally, all statistical comparisons were assessed using two-tailed paired t-tests (Appendix C).

3 Results

3.1 Segmentation

The CT scan images were first processed to obtain the patient's anatomical segmentation.

A total of 54 anatomical structures were segmented (Table A.1), including vascularized organs and LOARs.

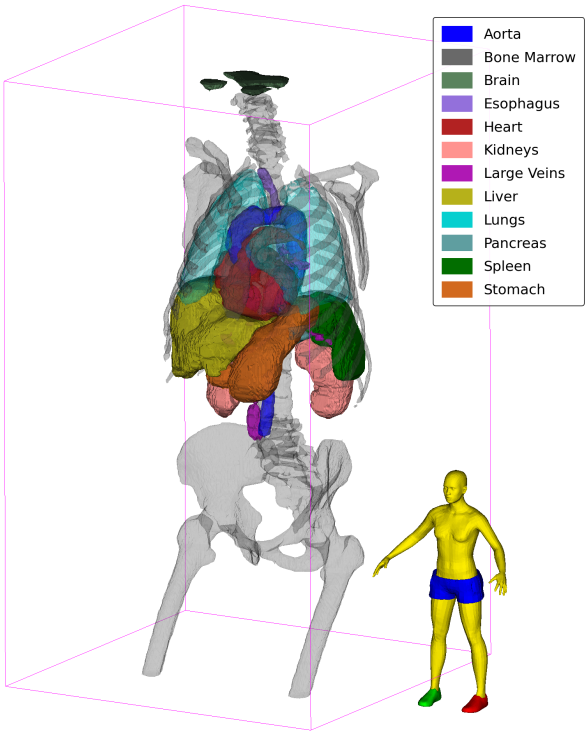

Figure 2: Organs segmented using TotalSegmentator. In total, 54 structures (Table A.1) were contoured, including LOARs and vascularized organs, and subsequently merged into groups and organs.

Two lung tumour volumes, representing T1- and T3-stage disease, were defined at similar locations in the right lung, in each of two copies of the CT scan.

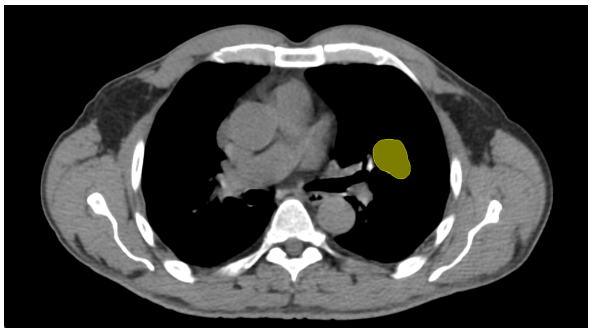

(a) Right lung tumour (8.93 cc) with largest diameter of 3.21 cm, representing a T1-stage case [19].

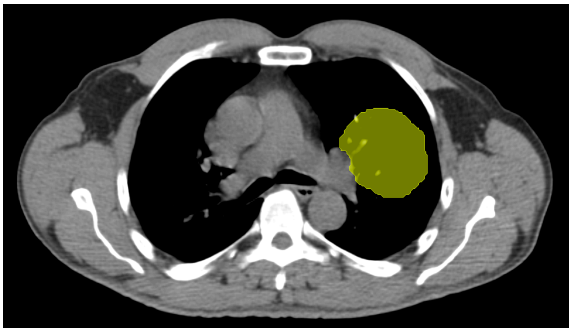

(b) Right lung tumour (132 cc) with largest diameter of 6.79 cm, representing a T3-stage case [19].

Figure 3: Manually drawn, similarly located right-lung tumours representing T1 (a) and T3 (b) stage lung cancer (size-based).

3.2 Irradiation

During radiation planning, aside from the change in guidelines for each plan, one difference between the plans was the monitor unit (MU) delivery per fraction, which was 547 MU for the MUHC plan and 836 MU for the LymphoTEC plan, since meeting the stricter LymphoTEC constraints required a higher MU delivery.

After attempting to optimize the irradiation of the smallest tumour with the LymphoTEC constraints, this case was discarded; it was not possible to improve the treatment plan, since the LymphoTEC constraints were already met when irradiated with the MUHC guidelines (the tumour being small, very little radiation was delivered to neighbouring organs). This observation suggests a dependence on tumour size within the scenarios considered in this work. The procedure was then carried out with the 132 cc (larger) tumour, and DVHs could be plotted.

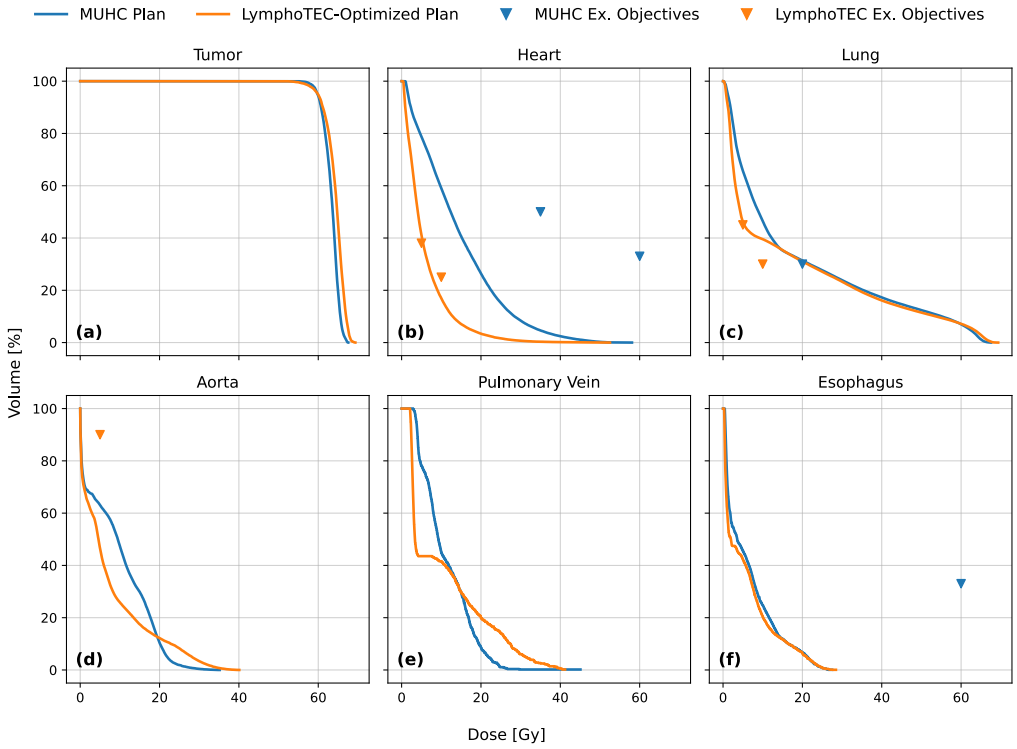

Figure 4: DVHs Comparison for vascular, neighbouring organs, and LOARs for two plans: one initial following the MUHC lung cancer guidelines, and one following stricter LymphoTEC guidelines. Dose-volume objectives for each plan and displayed organs are visualized; however, mean dose objectives are excluded as they cannot be plotted on DVHs in the same way.

For the heart and lungs (Figure 4 b,c), the stricter objectives lead to a decrease in the dose delivered to these organs. On the other hand, some trade-offs can be observed for the pulmonary vein and aorta (Figure 4 d,e), where the volume receiving lower doses decreased, but the volume receiving higher doses increased.

To assess whether tumour dose remained clinically acceptable after optimization, tumour dose metrics were extracted.

Table 3.1: Tumour dose metrics (voxel extrema and mean) expressed as a percentage of the prescription dose for the MUHC and LymphoTEC treatment plans.

Treatment plan	Minimum dose (%)	Mean dose (%)	Maximum dose (%)
MUHC	91.2	105.6	112.6
LymphoTEC	84.4	107.3	115.6

3.3 Blood Dose

By performing the HEDOS simulation, it was possible to acquire data on the dose delivered to BPs.

As the simulated particles entered the irradiation field, including the tumour and neighbouring organs, they absorbed radiation. Since each particle followed a unique trajectory through the irradiated volume, it accumulated a distinct absorbed dose over the course of the simulation. This enabled the construction of a per-fraction histogram of absorbed dose across all simulated BPs.

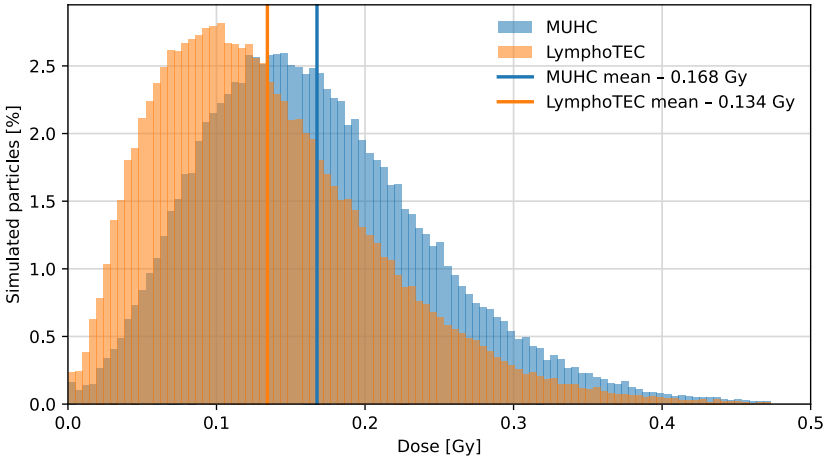

Figure 5: Blood dose histograms of simulated blood particles for the MUHC and LymphoTEC treatment plans, shown for a single Monte-Carlo resimulation of a single-fraction irradiation scenario. Each histogram was normalized such that the total area under the curve was 100% for each plan.

As shown in Fig. 5, the per-fraction blood dose distribution for the LymphoTEC plan is shifted toward lower absorbed doses when compared to the MUHC plan, showing a lower mean blood dose per fraction. These values over 12 runs were respectively (0.168 ± 0.001) Gy for the MUHC plan and (0.134 ± 0.001) Gy for the LymphoTEC plan, with the small standard error on the mean reflecting identical model parameters and repeated simulations reducing statistical noise.

Over the course of 30 fractions, the total cumulative blood dose was 5.04 Gy for the initial MUHC guidelines treatment, and 4.02 Gy for the optimized plan with LymphoTEC guidelines.

Since different organs have different levels of vascularization, their contribution to the absorbed blood dose varies. More vascularized organs, such as the heart and lungs, are more likely to contain circulating BPs and therefore contribute more to the absorbed dose. HEDOS allows these organ-specific contributions to be compared between treatment plans. While Fig. 5 shows the overall dose absorbed per simulated blood particle, Fig. 6 shows how each organ contributed to this total dose.

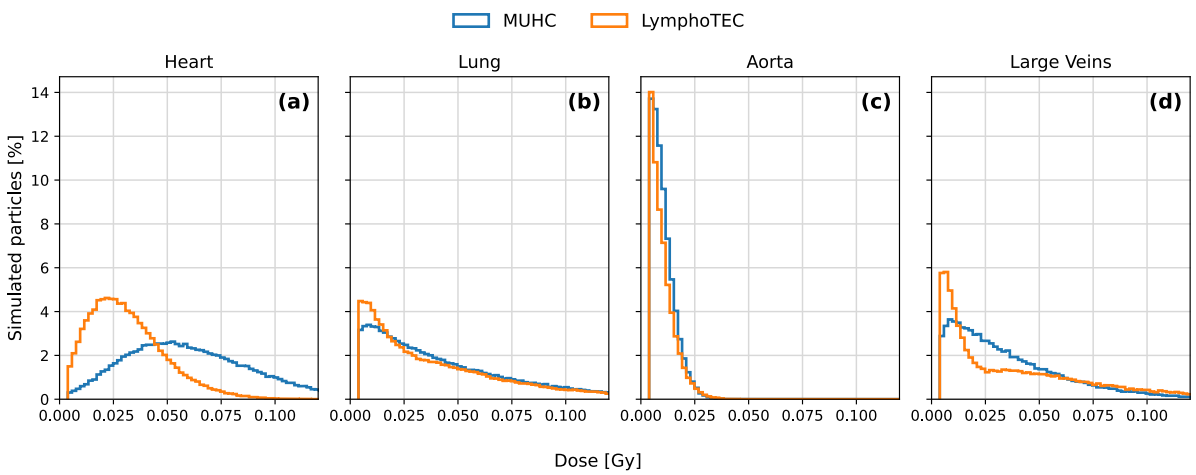

Figure 6: Organ-specific contributions to the total absorbed blood dose. Differences between organs reflect variations in vascularization and irradiation.

3.4 Lymphocyte Survival

Using the lymphocyte survival model defined in this work (Eq. 3), the predicted ALC evolution over the treatment course was simulated.

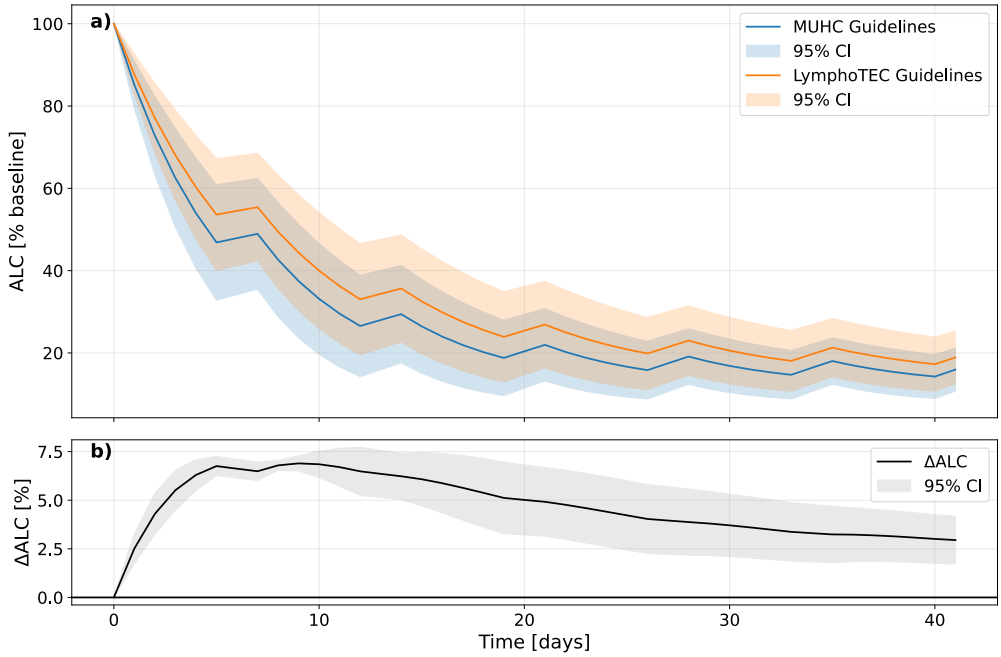

Figure 7: Absolute lymphocyte count evolution over 30 fractions. (a) ALC evolution for the initial and optimized treatment plans. The wide confidence interval is due to high biological variability in the lymphocyte radiosensitivity parameter. (b) Difference in ALC between the two plans over the course of treatment. Due to the paired nature of the data, the confidence interval narrows (see Appendix B for full details). Clinical lymphopenia thresholds are defined on absolute ALC values and are therefore not shown.

During the first 14 days of irradiation, the largest difference in ALC between the initial and

optimized plans, $|\Delta\text{ALC}|_{\max}$, occurred on day 9, with an improvement of 6.89% with respect to baseline (95% CI: 6.51–7.28%), corresponding to a relative improvement of 18.40% compared to the initial plan (95% CI: 17.37–19.43%). This difference was statistically significant ($p < 0.0001$, $\alpha = 0.05$).

At the lowest ALC, happening on the day of the last fraction, the difference in ALC between the initial and optimized plans, $|\Delta\text{ALC}_{\min}|$, was 3.01% compared to baseline (95% CI: 1.76–4.26%), corresponding to a relative improvement of 21.12% compared to the initial plan (95% CI: 12.34–29.89%), again indicating a statistically significant difference between the two plans ($p < 0.0001$, $\alpha = 0.05$).

4 Discussion

4.1 Analysis of Results

4.1.1 Segmentation

Thorough organ contouring is crucial when undertaking blood dose calculations, as it affects the precision and accuracy of the estimated blood dose. Precise organ contouring is required both to correctly identify which organs are being irradiated, and to determine the dose to each, particularly when performing replanning. Moreover, any irradiated organ that is not contoured does not contribute to the blood dose calculated by HEDOS, and could cause an underestimation of the total blood dose absorbed.

In this sense, this project builds upon the work of McCullum et al. [24], which included only a few organs, by incorporating more complete anatomical contouring, in an attempt to obtain more accurate and precise blood dose estimations. This work also enabled an automated and structured pipeline for CT input and three-dimensional organ mask output, allowing DICOM data from any CT to be used.

In this project, a single lung tumour and patient were used, yet the established pipeline allows contouring of over 100 structures from any CT input.

4.1.2 Irradiation

Upon optimization with the LymphoTEC constraints, the smaller of the two tumours had to be discarded due to the initial MUHC constraints yielding DVHs that already met the LymphoTEC guidelines, evincing that lymphocyte-sparing radiation therapy should potentially be given emphasis in specific larger-tumour cancer cases. When dealing with a single small tumour, irradiation can be more localized, resulting in a lower dose to neighbouring LOARs, where lymphocytes reside or are produced, as well as to vascularized organs through which lymphocytes transit in the bloodstream. Smaller tumours therefore raise two difficulties for lymphocyte-sparing treatment, despite being clinically favourable: they can complicate the task of optimization while also resulting in lower blood dose, leaving less room for further improvement.

Overall, lymphocyte-sparing optimization reduced blood dose mainly by decreasing the irradiation of highly vascularized organs such as the heart and lungs. At the same time, these stricter constraints caused some trade-offs for the aorta and pulmonary vein, where the volume receiving lower doses decreased, while the volume receiving higher doses increased. This indicates that the optimized constraints cause the dose to redistribute rather than lowering it for all structures.

With respect to the tumour, optimization slightly widened the range of delivered dose between the minimum and maximum values. Such changes could represent a cold spot and trade-off that should be assessed by clinicians to ensure that tumour coverage is not compromised.

4.1.3 HEDOS and Blood Dose

LymphoTEC guidelines stipulate that the estimated dose to immune cells (EDIC) should remain below 4–7 Gy, and that an EDIC greater than 4 Gy was found to be associated with a greater than 50% risk of grade 3 lymphopenia [12]. Therefore, despite the lower mean blood dose per fraction observed for the LymphoTEC plan, the cumulative blood dose over 30 fractions remained important for both treatments (5.04 Gy for MUHC and 4.02 Gy for LymphoTEC), indicating that both plans may still clinically induce lymphopenia.

The reduction in mean blood dose is consistent with the redistribution of organ-specific contributions to total blood dose. As it was lowered for the heart and large vessels, and because these structures are highly vascularized, even small changes in their irradiated volumes can have a measurable impact on the total blood dose.

4.1.4 Lymphocyte Survival

The optimized LymphoTEC-guideline-based plan resulted in a higher sparing throughout the treatment compared to the MUHC-guidelines-based plan. The highest benefit, $|\Delta\text{ALC}|_{\max}$, was observed early in the treatment on day 9 (18.40% relative sparing and 6.89% difference from baseline), suggesting that lymphocyte sparing was most impacted by the blood dose per fraction and not by a cumulative sparing effect over the treatment. These results align with the saturation model, in which a constant fraction of the ALC is assumed to be radio-resistant; as the ALC decreases over the course of treatment, the number of lymphocytes depleted at each fraction therefore decreased gradually.

Although the difference between the two plans decreased as the treatment progressed, the benefits of the stricter constraints were still significant at the lowest point, $|\Delta\text{ALC}_{\min}|$, (21.12% relative sparing, 3.01% difference from baseline), indicating that the stricter objectives were able to reduce lymphocyte depletion at its peak.

While these changes represent significant relative differences, the extent to which the lymphopenia grade could be different would be entirely dependent upon the baseline ALC. As each lymphopenia grade spans an interval of 200–300 lymphocytes per μL (Table 1.1), the percent difference could represent entirely different scenarios for a baseline of 1000 vs 2000 lymphocytes per μL.

Most importantly, delivery and simulation parameters, as well as irradiation methods, were kept

identical between plans, and observed differences can be attributed to the choice of planning constraints rather than to differences in treatment delivery.

4.2 Limitations, Sources of Error and Improvements

While these results are encouraging, possible improvements should be further investigated. As mentioned in the original HEDOS paper, the dynamical model relies in part on non-patient-specific assumptions. Therefore, future work should consider further personalizing the blood flow model based on clinical measurements.

The precision of organ contouring could also have introduced sources of error affecting both the optimization and blood dose estimation that could not be empirically measured. Consequently, future work should rely on clinical datasets, allowing validated contours to be used.

Moreover, this project only focused on a single hypothetical tumour located in the lungs and adjacent to the heart, two highly vascularized organs. The case explored might therefore overestimate the potential benefits of replanning achievable in actual clinical cases. Attempting replanning on a larger set of clinical cases, varying tumour location and size, would be required before drawing conclusions on the general achievability of lymphocyte-sparing approaches.

Data conversion from DICOM files to NumPy arrays also introduced difficulties when converting organ contours into voxel masks, as it led to the generation of degenerate polygons (i.e., contours too small for the resolution of the NumPy mask, resulting in the collapse of a 2D shape into a line). These shapes, totalling slightly under one per organ for 256 CT slices, had to be discarded to proceed with the simulation. Although the impact of this removal on the final estimated dose is expected to be minimal, as the discarded areas were negligible, addressing this issue would be valuable to avoid disregarding data.

Finally, if future work were to rely on TotalSegmentator again, although most major organs relevant to this case were contoured in this project, some minor ones could also be included, as well as organs not irradiated here but relevant in other treatment scenarios. The full capability of the contouring algorithm was not explored, as performing a complete segmentation would require a more powerful computer.

4.3 Outlooks

Whereas this project only considered a single case, and since the pipeline allows for simulation of many different cancer types, it would be relevant to extend this analysis to multiple patients, different treatment modalities, and the use of clinical contouring. When extending this approach to other cases, tumour coverage must continue to be verified to ensure that lymphocyte sparing does not compromise the primary treatment objective.

5 Conclusion

This project enabled the implementation of a complete evaluative pipeline for lymphocyte-sparing radiation therapy treatment planning, starting from a CT scan and automatic organ segmentation, followed by treatment planning using two different irradiation plans. A HEDOS simulation was then performed to estimate the hematological dose, which was subsequently used to predict ALC evolution and allow for comparison between the two plans.

More precisely, in the case of a large single lung tumour explored, a significant improvement in lymphocyte survival was observed with the stricter LymphoTEC guidelines versus MUHC ones.

As this project offers a preliminary investigation of lymphocyte-sparing radiation therapy, it highlights the potential for more personalized treatment planning. This aligns with a broader move in the medical field toward personalized care; prior to 2015, ALC was largely considered a research interest in radiation oncology and was not routinely included in clinical trials [25].

Acknowledgements

I would like to thank Douaa El Abiad and Odette Rios Ibacache for their precious help and for patiently answering my many questions.

References

[1] Sender R, Weiss Y, Navon Y, Milo I, Azulay N, Keren L, et al. The total mass, number, and distribution of immune cells in the human body. Proc Natl Acad Sci U S A. 2023 Oct;120(44):e2308511120.

[2] Bonilla FA, Oettgen HC. Adaptive Immunity. J Allergy Clin Immunol. 2010 Feb;125(2):S33–S40.

[3] Trepel F. Number and Distribution of Lymphocytes in Man. A Critical Analysis. Klin Wochenschr. 1974 Jun;52(11):511–515.

[4] Paganetti H. A Review on Lymphocyte Radiosensitivity and Its Impact on Radiotherapy. Front Oncol. 2023 Aug;13:1201500.

[5] Valentin J. Basic Anatomical and Physiological Data for Use in Radiological Protection: Reference Values: ICRP Publication 89. Ann ICRP. 2002 Sep;32(3-4):1–277.

[6] Pham TN, Coupey J, Thariat J, Valable S. Lymphocyte Radiosensitivity: An Extension to the Linear-Quadratic Model? Radiother Oncol. 2024 Sep;198:110406.

[7] National Cancer Institute. CTCAE and AE Reporting - NCI; 2025. https://dctd.cancer.gov/research/ctep-trials/for-sites/adverse-events.

[8] Ellsworth SG. Field Size Effects on the Risk and Severity of Treatment-Induced Lymphopenia in Patients Undergoing Radiation Therapy for Solid Tumors. Adv Radiat Oncol. 2018 Oct;3(4):512–519.

[9] The Circulatory System. In: Antman SS, Marsden JE, Sirovich L, Keener J, Sneyd J, editors. Mathematical Physiology. vol. 8/2. New York, NY: Springer New York; 2009. p. 471–522.

[10] Damen PJJ, Kroese TE, Van Hillegersberg R, Schuit E, Peters M, Verhoeff JJC, et al. The Influence of Severe Radiation-Induced Lymphopenia on Overall Survival in Solid Tumors: A Systematic Review and Meta-Analysis. Int J Radiat Oncol Biol Phys. 2021 Nov;111(4):936–948.

[11] Lambin P, Lieverse RIY, Eckert F, Marcus D, Oberije C, Van Der Wiel AMA, et al. Lymphocyte-Sparing Radiotherapy: The Rationale for Protecting Lymphocyte-rich Organs When Combining Radiotherapy With Immunotherapy. Semin Radiat Oncol. 2020 Apr;30(2):187–193.

[12] Venkatesulu B, Giridhar P, Pujari L, Chou B, Lee JH, Block AM, et al. Lymphocyte Sparing Normal Tissue Effects in the Clinic (LymphoTEC): A Systematic Review of Dose Constraint Considerations to Mitigate Radiation-Related Lymphopenia in the Era of Immunotherapy. Radiother Oncol. 2022 Dec;177:81–94.

[13] Molloy JA. Statistical Analysis of Dose Heterogeneity in Circulating Blood: Implications for Sequential Methods of Total Body Irradiation. Med Phys. 2010 Nov;37(11):5568–5578.

[14] Jin JY, Mereniuk T, Yalamanchali A, Wang W, Machtay M, (Spring)Kong FM, et al. A Framework for Modeling Radiation Induced Lymphopenia in Radiotherapy. Radiother Oncol. 2020 Mar;144:105–113.

[15] Shin J, Xing S, McCullum L, Hammi A, Pursley J, Correa CA, et al. HEDOS—a Computational Tool to Assess Radiation Dose to Circulating Blood Cells during External Beam Radiotherapy Based on Whole-Body Blood Flow Simulations. Phys Med Biol. 2021 Aug;66(16):164001.

[16] Vallières M, Freeman CR, Skamene SR, El Naqa I. A Radiomics Model from Joint FDG-PET and MRI Texture Features for the Prediction of Lung Metastases in Soft-Tissue Sarcomas of the Extremities. The Cancer Imaging Archive; 2015.

[17] Isensee F, Jaeger PF, Kohl SAA, Petersen J, Maier-Hein KH. nnU-Net: A Self-Configuring Method for Deep Learning-Based Biomedical Image Segmentation. Nat Methods. 2021 Feb;18(2):203–211.

[18] Wasserthal J, Breit HC, Meyer MT, Pradella M, Hinck D, Sauter AW, et al. TotalSegmentator: Robust Segmentation of 104 Anatomic Structures in CT Images. Radiol Artif Intell. 2023 Sep;5(5):e230024.

[19] Detterbeck FC. The Eighth Edition TNM Stage Classification for Lung Cancer: What Does It Mean on Main Street? J Thorac Cardiovasc Surg. 2018 Jan;155(1):356–359.

[20] Ethanio12345. HEDOS; 2021. [Internet; cited 2026 Jan 7]. https://github.com/ethanio12345/hedos.

[21] Lowekamp BC, Chen DT, Ibáñez L, Blezek D. The Design of SimpleITK. Front Neuroinform. 2013;7:45.

[22] Mason D. Pydicom: An Open Source DICOM Library. Med Phys. 2011 Jun;38(6Part10):3493–3493.

[23] Radiation Oncology Department. Radiation Oncologist Treatment Planning Guidelines for Lung Cancer. Montreal, QC, Canada; 2024. Institutional treatment planning guidelines; 30-fraction regimen.

[24] McCullum L, Shin J, Xing S, Beekman C, Schuemann J, Hong T, et al. Predicting Severity of Radiation Induced Lymphopenia in Individual Proton Therapy Patients for Varying Dose Rate and Fractionation Using Dynamic 4-Dimensional Blood Flow Simulations. Int J Radiat Oncol Biol Phys. 2023 Aug;116(5):1226–1233.

[25] Grossman SA, Ellsworth S, Campian J, Wild AT, Herman JM, Laheru D, et al. Survival in Patients With Severe Lymphopenia Following Treatment With Radiation and Chemotherapy for Newly Diagnosed Solid Tumors. J Natl Compr Canc Netw. 2015 Oct;13(10):1225–1231.

A Segmented Organs and Structures

Table A.1: Segmented Organs and Structures

Organ System	**Structure**
Head	brain
Cardiothoracic	heart
	esophagus
	pulmonary vein
	left lung lobes (2)
	right lung lobes (3)
Abdominal	liver
	spleen
	stomach
	pancreas
	kidneys (2)
Skeletal (Thorax)	sternum
	claviculae (2)
	scapulae (2)
	vertebrae body
	intervertebral discs
	ribs (24)
Skeletal (Pelvic)	sacrum
	hips (2)
	femurs (2)
Vascular	aorta
	inferior vena cava
	portal + splenic vein

B Uncertainty Propagation for ALC(t)

Two plans were compared: Initial (Init.) and Optimized (Opt.). Each plan was simulated n times. Every simulation run gave an ALC curve $\mathrm{ALC}_{\mathrm{run}}^{(\mathrm{Plan})}(t)$.

1. Statistical uncertainty

The mean ALC for a plan was

$$\bar{ALC}^{(\mathrm{Plan})}(t) = \frac{1}{n}\sum_{i=1}^{n} \mathrm{ALC}_{\mathrm{i}}^{(\mathrm{Plan})}(t).$$

Uncertainty from run-to-run variation was

$$\sigma_{\mathrm{stat}}^{(\mathrm{Plan})}(t) = \frac{\text{standard deviation across runs}}{\sqrt{n}}.$$

2. Biological uncertainty

The model used parameters μ and S_{sat} with known population uncertainties. Their effect was estimated by recomputing the ALC curve with

$$\mu \pm \sigma_\mu, \qquad S_{\mathrm{sat}} \pm \sigma_S.$$

The resulting changes gave the biological uncertainty:

$$\sigma_{\mathrm{bio}}^{(\mathrm{Plan})}(t) = \sqrt{(\text{sensitivity to } \mu)^2 + (\text{sensitivity to } S_{\mathrm{sat}})^2}.$$

3. Difference between plans

For each run:

$$\Delta\mathrm{ALC}_{\mathrm{run}}(t) = \mathrm{ALC}_{\mathrm{run}}^{(\mathrm{Opt.})}(t) - \mathrm{ALC}_{\mathrm{run}}^{(\mathrm{Init.})}(t).$$

Statistical uncertainty was evaluated from the standard deviation of these within-run differences, which inherently accounts for shared variability between plans (paired data).

The same steps (mean, statistical uncertainty, biological uncertainty) were applied to the difference curve.

4. Total uncertainty

Total uncertainty combines statistical and biological parts:

$$\sigma_{\mathrm{tot}}(t) = \sqrt{\sigma_{\mathrm{stat}}(t)^2 + \sigma_{\mathrm{bio}}(t)^2}.$$

The shaded bands in the figures correspond to the 95% intervals:

$$\text{mean} \pm 1.96\,\sigma_{\mathrm{tot}}(t).$$

C Statistical Tests

Statistical comparisons between the initial (MUHC) and optimized (LymphoTEC) treatment plans were performed using two-tailed paired t-tests.

Each HEDOS run produced one predicted ALC trajectory for each plan, using identical biological parameters. As a result, outcomes from the two plans were naturally paired by simulation run.

Two paired comparisons were evaluated:

- The drop in ALC from baseline at the end of treatment (Day 40).
- The maximum ALC drop during the early treatment window (Days 0–14).

For each one, the difference between plans was computed per run and tested against a null hypothesis of zero mean difference. Statistical significance was assessed at the $\alpha = 0.05$ level.